ADVANCED FUNCTIONAL MATERIALS
www.afm-journal.de

Electrospun Photocrosslinkable Hydrogel Fibrous Scaffolds for Rapid In Vivo Vascularized Skin Flap Regeneration

Xiaoming Sun, Qi Lang, Hongbo Zhang, Liying Cheng, Ying Zhang, Guoqing Pan, Xin Zhao, Huilin Yang, Yuguang Zhang, Hélder A. Santos,* and Wenguo Cui**

Distal necrosis of random skin flap is always clinical problematic in plastic surgery. The development of 3D functional vascular networks is fundamental for the survival of a local random skin flap. Herein, an effective technique on constructing 3D fibrous scaffolds for accelerated vascularization is demonstrated using a photocrosslinkable natural hydrogel based on gelatin methacryloyl (GelMA) by electrospinning. It is found that the ultraviolet (UV) photocrosslinkable gelatin electrospun hydrogel fibrous membranes exhibit soft adjustable mechanical properties and controllable degradation properties. Furthermore, it is observed that the optimized hydrogel scaffolds can support endothelial cells and dermal fibroblasts adhesion, proliferation, and migration into the scaffolds, which facilitates vascularization. Importantly, a rapid formation of tubes is observed after 3 d seeding of endothelial cells. After GelMA fibrous scaffold implantation below the skin flap in a rat model, it is found that the flap survival rate is higher than the control group, and there is more microvascular formation, which is potentially beneficial for the flap tissue vascularization. These data suggest that GelMA hydrogels can be used for biomedical applications that require the formation of microvascular networks, including the development of complex engineered tissues.

1. Introduction

Local random skin flaps, also called subdermal plexus skin flaps, are commonly used for repairing and reconstructing tissue defects in plastic surgery.[1,2] However, due to the limited length-to-width ratio of the skin flap or local and systemic metabolic disease, such as diabetes mellitus, distal necrosis is always a clinical problem. These reasons would result in delayed wound healing and the possibility of a second operation, which may limit the applications of local random skin flaps in clinic.[3,4] To date, although the exact pathogenic mechanism of skin flap necrosis remains unknown, ischemia–reperfusion injury, inadequate blood supply, and hemodynamic injury are suspected to be the principal factors in this complication.[5] Therefore, increased blood vessel density and promoted blood flow will contribute to random skin flap survival. Furthermore, it is reported that the revascularization from the wound bed itself is more important compared with that originating from the edges of the skin flap,[6] thus efforts to stimulate vascularization from the wound bed and promote blood supply for improving flap survival are still standing.

Numerous studies have been carried out to improve the local perfusion and promote vascularization for many years. Recent advances in tissue engineering, various kinds of 3D scaffolds with functional cells, or growth factors have been implanted into animal body for improving vascularization.[7,8] However, these scaffolds with obvious 3D structure, which remain in the body for a long time, can cause

Dr. X. Sun, Dr. L. Cheng, Prof. Y. Zhang, Prof. Y. Zhang
Department of Plastic and Reconstructive Surgery
Shanghai Ninth People's Hospital Affiliated
to Shanghai Jiaotong University of Medicine
639 Zhi Zao Ju Road, Shanghai 200011, China
E-mail: zhangyg18@126.com

Dr. Q. Lang
Institute of Biomedicine and Biotechnology
Shenzhen Institutes of Advanced Technology
Chinese Academy of Sciences
Shenzhen, Guangdong 518055, P. R.China

Prof. H. Zhang, Prof. H. A. Santos
Division of Pharmaceutical Chemistry and Technology
Faculty of Pharmacy
University of Helsinki
Helsinki FI-00014, Finland
E-mail: helder.santos@helsinki.fi

Dr. G. Pan, H. Yang, Prof. W. Cui
Department of Orthopedics
the First Affiliated Hospital of Soochow University
Orthopedic Institute
Soochow University
708 Renmin Road, Suzhou, Jiangsu 215006, China
E-mail: wgcui@hotmail.com

Dr. X. Zhao
School of Life Science and Technology
Xi'an Jiaotong University
Xi'an, Shaanxi 710049, P. R. China

Prof. H. Zhang
Department of Pharmaceutical Science
Åbo Akademi University
Turku Fi-20520, Finland

DOI: 10.1002/adfm.201604617

a significant foreign body reaction in the local subcutaneous tissue, as well as can cause fibrosis and lead to the bad vascularization. This is not suitable for application in the repair of random skin flap, because local skin flaps are fed by the direct cutaneous artery terminal branches without regard to their inherent vascularization. Additionally, the early stage after flap harvested is a critical time for revascularization to keep the skin flap survival.[6,9,10] Therefore, how to fabricate a rapid vascularized biological scaffold remains challenging.

Biological scaffold is an important factor to promote vascularization, which mainly provides skeleton support for cell adhesion and is conductive to the formation of lumen. Recently, electrospinning technology has a wide range of applications in creating extracellular matrix (ECM)-mimicking ultrafine fibrous membranes with fiber diameters ranging from nanometers to micrometers. Moreover, their ECM-mimicking structure is conductive to cell adhesion and substances exchange, which makes electrospun fibrous membranes intensively studied in promoting vascularization. Many studies reported that 2D or 3D structures of electrospinning fibers meshes were fabricated using poly(L-lactic acid) or poly(ε-caprolactone) for vascularization. But in vitro results indicated that endothelial cells can only grow on the surface of the fiber mesh due to the small pore size, making it difficult to construct 3D vasculature in the scaffolds.[11,12] In addition, stiffness material is not suitable for the soft tissue regeneration, which would cause severe inflammatory response in vivo.[9] Therefore, fabrication of a biocompatible electrospinning fiber scaffolds with proper pore size for cells migration mimicking the properties of skin is urgently needed.

Hydrogels as biomaterials have been widely investigated for numerous medical applications. Because of their high water content and elastic similarities between hydrogels and soft tissues in the body, hydrogels are particularly used for tissue engineering, wound healing, and as bioadhesives.[13–16] From the above description, we put forward the concept of electrospinning hydrogel fibers that possess dual properties of electrospun fibrous nanostructure and hydrogel softness, which is expected to allow cell migration into the scaffolds to construct 3D microvascular structures. Hence, soft electrospun hydrogel fibers have potential to be ideal biomaterial scaffold for promoting vascularization. Therefore, we hypothesize that such hydrogel fibrous membranes fabricated by electrospinning are conducive to: (1) endothelial cell adhesion and growth; (2) tubulogenesis; (3) skin flap adhesion of the wound bed; and (4) the formation of microvasculature, which will increase the number of capabilities to aid blood supply, and sequentially enhancing the survival rate of random skin flap after implantation.

Gelatin methacryloyl (GelMA) hydrogel, which is fabricated by incorporating methacrylate groups to the amine-containing side groups of gelatin, is a photocrosslinkable hydrogel. Modification of gelatin with photocrosslinkable methacryloyl groups maintains the unique properties of gelatin, but additionally endows the material with solidification from liquid to solid permanently via chemical reaction of the methacryloyl groups.[17,18] Furthermore, by varying the methacryloyl modification degree (i.e., to change the polymer crosslinking density for controlling the hydrogel network structure), its mechanical, degradation, and biological properties can be easily tuned.[19] Moreover, it has been reported that GelMA hydrogel could support human progenitor cell-based formation of vascular networks both in vitro and in vivo.[20]

Therefore, in this study, we synthesize an ultraviolet (UV) photocrosslinkable gelatin hydrogel and then fabricate the hydrogel nanofibrous membrane by electrospinning, which possess the property of absorbing water in a liquid environment. Furthermore, the photocrosslinkable gelatin electrospun hydrogel fibrous membranes exhibit soft adjustable mechanical and controllable degradation properties. Here, we investigated the morphology, water retention, and mechanical and degradation properties of the fibrous membranes in vitro. Additionally, the ability of GelMA nanofibrous membrane for cellular adhesion, proliferation, and secretion, as well as vascularization, was also evaluated in vitro. In order to explore the potential of the GelMA nanofibrous membrane for promoting random skin flap survival applications, in vivo blood supply and vascularization were also investigated in a rat model.

2. Results and Discussion

Loss of blood supply resulting in tissue ischemia is one of the leading causes of tissue defect in the developing world.[21] Tissue engineering is a promising approach to treat tissue regeneration. The generation of 3D vascular networks that can provide oxygen and nutrients to sustain cell viability is one of the most active areas of research in tissue engineering.[22,23] Because of the characteristics of controllable degradation time with the angiogenic process, mild preparation conditions, and structurally similar to the tissue ECM, hydrogels are especially suitable for the vascularization of tissue engineering scaffolds.[24,25] Many kinds of natural collagen-based hydrogels and Matrigel have been shown for their favorable microenvironments for angiogenesis. But, because of different sources of species or poor mechanical stability, they are not suitable for tissue engineering applications in clinic.[26–29] Moreover, the GelMA hydrogel fabricated by chemically modified gelatin with methacrylic anhydride (MA) before photoinitiated radical polymerization also has the advantages of being biocompatible, non-cytotoxic, biodegradable, and nonimmunogenic.[19,30] In addition, a variety of studies have been reported that GelMA hydrogels were successfully used for the development of 3D vascular networks. For example, Chen et al.[20] indicated that GelMA hydrogels containing endothelial colony-forming cells and mesenchymal stem cells can act as the scaffolds for vascular morphogenesis in vitro. In this study, we fabricated GelMA electrospun hydrogel fibrous scaffolds by electrospinning the GelMA solution synthesized by the direct reaction of gelatin with MA under UV light exposure, which were made as the 3D gel matrices for rapid vascularization in vivo.

2.1. Fabrication of Crosslinked Gelatin and GelMA Electrospun Fibers

To form electrospun fibrous hydrogel for 3D tissue regeneration, we first synthesized photocrosslinkable GelMA prepolymer by reacting methacrylic anhydride with gelatin.

Adv. Funct. Mater. 2016,
DOI: 10.1002/adfm.201604617

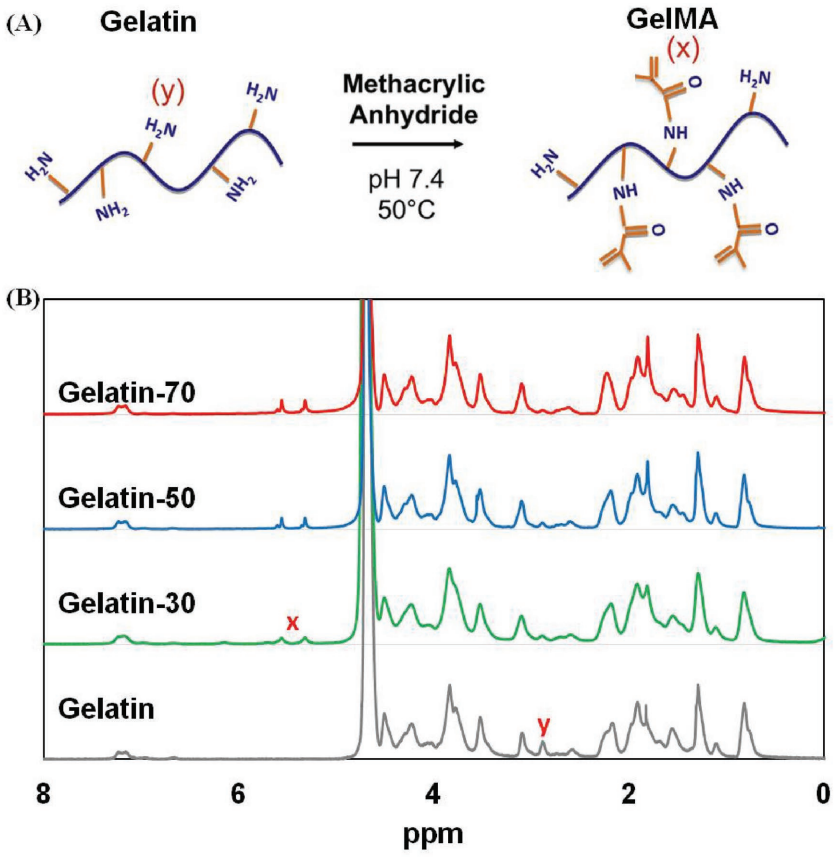

Figure 1. A) Synthesis of GelMA: Gelatin containing primary amine groups were reacted with methacrylic anhydride (MA) to add methacrylate pendant groups, and then the methacrylated gelatin was crosslinked using UV irradiation to create a hydrogel network. B) The NMR spectrum of synthesized GelMA. The gelatin component was modified to contain methacryloyl groups (Gelatin-30, Gelatin-50, and Gelatin-70), which formed crosslinked GelMA networks upon light exposure.

^{1}H NMR analyses confirmed that the synthesized GelMA prepolymer had 30%, 50%, and 70% methacryloyl modification (**Figure 1**), which is consistent with a previous report.[19] Therefore, three types of GelMA were fabricated using this method for obtaining different hydrogel fibers. The prepolymer solution (100 mg GelMA in 1 mL hexafluoro-2-propanol (HFIP)) was subject to electrospinning and UV exposure in photoinitiator (PI) solution for 30 min to fabricate the nanofibrous scaffolds (**Figure 2**B), and the crosslinked GelMA fibers were then subject to de-ionized (DI) water wash to remove the excess of photoinitiator. Electrospinning gelatin fibers (control) used the same procedure as described above and the electrospun fibers were chemically crosslinked using glutaraldehyde (10 mL glutaraldehyde•500 mL^{-1} ethanol) overnight. Finally, the excessive glutaraldehyde was removed using glycine (7.5 g per 500 mL of DI water).

2.2. Morphology of Fibrous Scaffolds

The microscopic morphologies of crosslinked gelatin and GelMA nanofibers were examined using scanning electron microscopy (SEM). As shown in Figure 2A,C, both kinds of fibers were well formed with randomly aligned and uniform shape, no matter if before or after soaking in phosphate buffered saline (PBS) for 24 h. The diameter of crosslinked gelatin fibers was 1.52 ± 0.36 µm (Figure 2A), while the diameter of GelMA fibers was 1.36 ± 0.27 µm (Figure 2C). There was no statistical significance between them. However, after 24 h incubation in PBS, the diameter of GelMA fibers increased to 2.18 ± 0.52 µm, while the crosslinked gelatin fiber only increased to 1.76 ± 0.45 µm (Figure 2D,E). Compared to the percentage diameter change of two kinds of fiber, the results revealed that GelMA fiber had a better water swelling property. In addition, it is worth noting that after incubating in PBS for 24 h, highly porous matrix architecture was found in the GelMA mat, while porous structure of crosslinked gelatin was not obvious. By simple methacrylate modification, it has been reported that the porosity of GelMA hydrogel can be tuned to achieve a desirable mechanical robustness without compromising the cellular biocompatibility.[31] Moreover, porosity is the characteristic of an ideal scaffold for cell culture purpose, which is beneficial for cell infiltration and efficient exchange of nutrients.[32]

2.3. Physical Characteristics of the Electrospun Fibrous Scaffolds

Ideal 3D-engineered matrices for vascularization should be constructed with the important parameters of appropriate water permeability and sorption. It was reported that higher permeability and sorption were beneficial to transport nutrients and wastes, which was good for cell survivability growth on the fibers and retention tissue fluid containing growth factors for vascularization.[33]

The swelling characteristics of a network are important in various applications as these had substantial effect on the physical properties of hydrogel. In our study, the changes in the mass swelling ratio of crosslinked gelatin and GelMA fiber mats were investigated (**Figure 3**A). GelMA fiber mats absorbed almost six times of own weight in PBS and then steadily declined in weight to about 4.0 times of the beginning weight after 5 d. Fibrous crosslinked gelatin scaffolds followed a similar trend, but have slightly reduced ability to absorb water (maximal sorption of 520%), and the final percentage weights after 5 d were 410%.

Two kinds of scaffolds permeability were recorded every 5 min for half an hour of the permeability test, as shown in Figure 3B. The permeability was calculated at each time point. Both kinds of scaffolds' permeability exhibited very little change over the course of time. Mean permeability was 2130 ± 160 L m^{-2} h^{-1} atm^{-1}, 1580 ± 110 L m^{-2} h^{-1} atm^{-1}, and 810 ± 90 L m^{-2} h^{-1} atm^{-1} for GelMA-30, GelMA-50, and

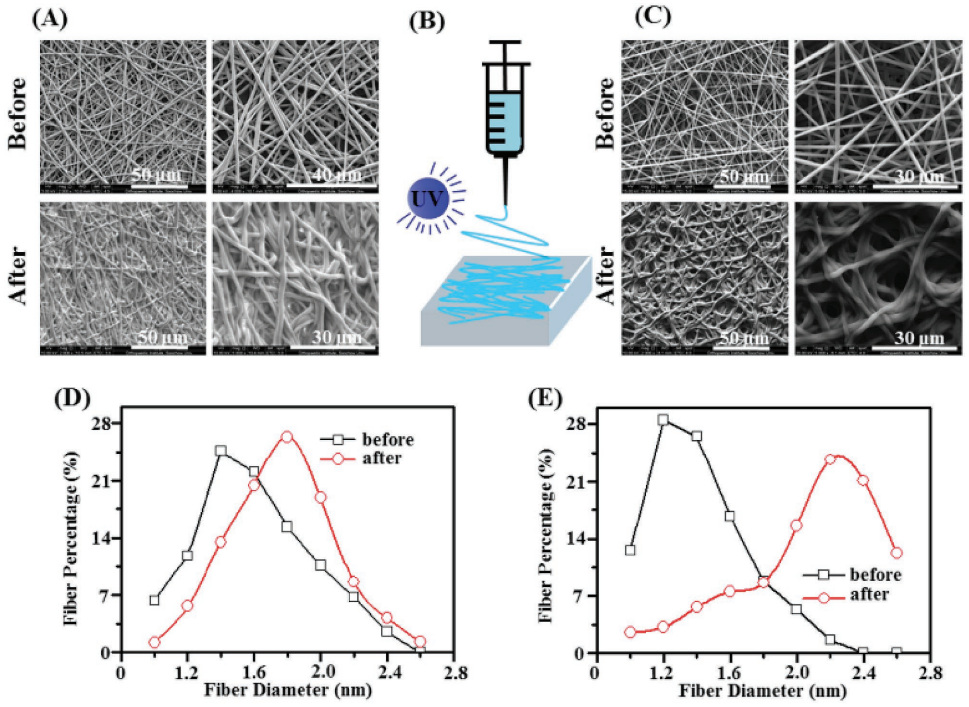

Figure 2. Fabrication and morphology of GelMA nanofibrous mats. A) The morphology of electrospun fibers of crosslinked gelatin before and after 24 h in PBS. B) Schematic diagram of electrospinning for fabricating GelMA fibers. C) The morphology of electrospun fibers of GelMA before and after 24 h in PBS. D) Fiber diameter of crosslinked gelatin changes after soaking PBS. E) Fiber diameter of GelMA changes after soaking PBS.

GelMA-70 fibrous scaffolds, and 680 ± 85 L m^{-2} h^{-1} atm^{-1} for gelatin fibrous scaffolds. The water permeability and sorption studies showed significant differences between crosslinked gelatin and GelMA groups. The water permeability and sorption of GelMA fibers were obviously better than crosslinked gelatin fibers. Such ability to maintain the hydration allows for the maintaining of significant amounts of growth factors for angiogenesis on wound bed.

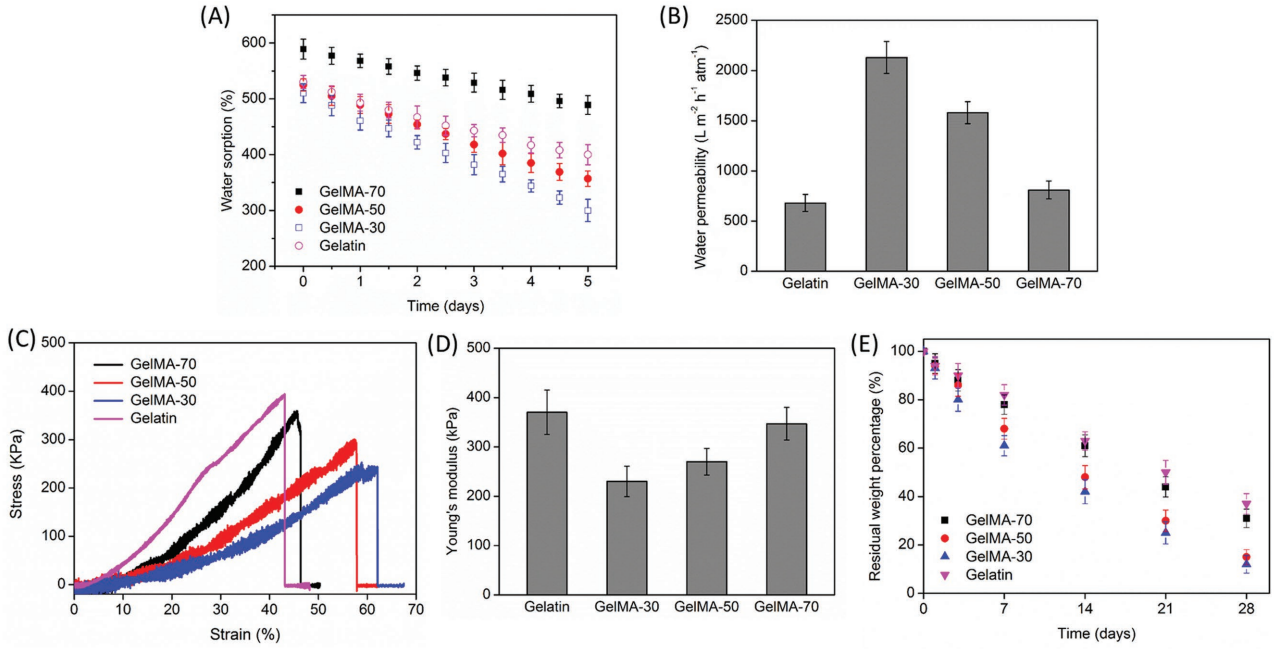

Figure 3. Physical characteristics of the electrospun fibrous scaffolds. A) Swelling properties of GelMA and crosslinked gelatin fibrous scaffolds. B) Water permeability of GelMA and crosslinked gelatin fibrous scaffolds. C,D) Mechanical properties of GelMA and crosslinked gelatin fibrous scaffolds. E) Degradation of GelMA and crosslinked gelatin fibrous scaffolds in vitro.

Adv. Funct. Mater. **2016**,
DOI: 10.1002/adfm.201604617

The tissue engineering scaffolds with structural and biochemical properties, such as mechanical properties and degradation rates, which are similar to the native tissues, are conducive to the formation of vascularization in vivo.[34,35] Moreover, various studies have shown that softer matrices could improve vessel formation.[36,37] Both kinds of electrospun scaffolds underwent mechanical testing after fully hydrated at 37 °C. Figure 3C,D shows the results of stress–strain curves of two different samples. Generally, it can be seen that the two kinds of materials displayed typical stress–strain curves. However, the crosslinked gelatin scaffold showed the higher tensile strength but lower longation at break compared with GelMA scaffold. Young's modulus, tensile strength, and elongation at break were found to be influenced by the scaffold material. GelMA scaffolds appeared more flexible/compliant (with slightly lower Young's modulus and tensile strength) compared to the control crosslinked gelatin scaffolds. GelMA-based scaffolds also exhibited a significant increase in the elongation at break (65%), possibly due to the increased chain length and decreased proportion of the crosslinkers (due to the 30%–70% methacryloyl modification in GelMA) compared to that in crosslinked gelatin, making the material more elastic and providing superior break elongation. Thus, our stress–strain curves results showed that for the two different samples, mechanical strength of crosslinked gelatin fiber was higher compared to GelMA; however, the two kinds of material displayed typical stress–strain curves, both of which can meet the requirements of tissue engineering materials. Particularly, it has been known that softer hydrogels could promote more extensive vascular networks formation.[38,39]

Degradation is one of the important characteristics of biological tissue engineering material. Next, we tested the GelMA fibrous scaffold degradability in vitro by measuring the percentage of weight loss. As Figure 3E shows, an initial relatively fast mass loss of almost 22%, 32%, and 39% for GelMA-30, GelMA-50, and GelMA-70, and 18% of crosslinked gelatin over the first 7 d was observed, followed by a more gradual loss to 69%, 85%, and 88% for GelMA-30, GelMA-50, and GelMA-70, and 63% of the initial weight of crosslinked gelatin fibrous scaffolds by day 28. Considering various properties, such as mechanical properties, degradation, and sorption rate synthetically, we have chosen crosslinked gelatin and GelMA as test samples for further biological evaluation in vitro and in vivo. The biomaterials of which the degradation rate is in line with the vascularization process are more conducive to tissue repair. In vitro, the GelMA fibrous scaffold exhibited faster degradation rate as compared to the crosslinked gelatin fibrous scaffold. This is consistent with the degradation situation in vivo (Figure 8E).

2.4. Cytocompatibility of Electrospun Hydrogel Fibrous Membranes

The ability of cells to survive and grow is of fundamental importance for tissue development. To evaluate the biocompatibility of the electrospun hydrogel fibrous membranes with human dermal fibroblasts (HDFs) and human umbilical vein endothelial cells (HUVECs), the cell viability and metabolic activity were assessed using the Live/Dead analysis and CCK-8 assay, respectively. HDF and HUVEC viability was calculated by quantifying the live and dead cells adhered to the hydrogel fibrous membranes (**Figure 4**A,B). Live/Dead analysis showed that HDFs and HUVECs were viable on crosslinked gelatin membranes with over 80% viability after culture for 1 d, but HUVEC viability slightly reduced. In addition, both kinds of cells seeded on the GelMA hydrogels remained more than 85% viable for 1 d culturing, and greater than 90% for 3 d culturing. Cell metabolism was determined utilizing CCK-8 assay. It was found that the metabolic activity of both kinds of cells seeded on the membranes increased with time. At day 1, HDF metabolic activity was not significantly different on the crosslinked gelatin and GelMA membranes, while HUVECs on the GelMA membrane had higher metabolism than on the crosslinked gelatin membrane ($p < 0.05$). By day 3, for both HDFs and HUVECs, CCK-8 values within GelMA groups were significantly greater than the gelatin group (Figure 4C). Many reports have demonstrated that degradation products, methacryloylated amino acid derivatives or methacrylic acid, are small molecules and relatively non-toxic, which can easily be excreted directly or after entry and exit from various metabolic pathways.[40,41] Overall, the cellular suitability of GelMA fibrous scaffold was better than crosslinked gelatin fibrous scaffold in vitro.

SEM images of the seeded HDFs and HUVECs on crosslinked gelatin and GelMA hydrogel membranes at day 3 were also presented, respectively. Both HDFs and HUVECs appeared to attach well on the gelatin and GelMA membranes, but HDFs and HUVECs on electrospun crosslinked gelatin membranes formed spherical or spindle morphology with plenty of filiform pseudopodia linked to the fibers (**Figure 5**A-a,c). HDFs showed fiber or flatted morphology after 3 d of culture on the GelMA membrane (Figure 5A-b). At day 3, HUVECs adhered to the fiber tightly and differentiated into a fibrous morphology connected to each other (Figure 5A-d). Furthermore, it revealed that the number of cells grown on the membranes increased with time. At days 1 and 3, cells were more abundant on the GelMA membranes compared with the crosslinked gelatin membrane (Figure 5B). As shown in Figure 5B, compared with cells grown on crosslinked gelatin membrane, HDFs grown on GelMA surfaces showed themselves more elongated with higher numbers of filamentous and interconnected projections. At the same time, it was noticed that after 3 d of culturing, HUVECs on the GelMA membranes connected with each other to form tube structures (Figure 5B).

To conclude, in this study, after chemically modification with methacryloyl substituent groups, GelMA fibers were photocrosslinked by exposure to UV light at mild conditions; however, gelatin was chemically crosslinked with glutaraldehyde. Also, it has been indicated that the functional amino acid motifs, such as arginyl-glycyl-aspartic acid (RGD) motifs, will not be significantly influenced due to MA, which ensures GelMA with good cell adhesive properties. In addition, a recent study also clearly demonstrated that strong adhesion between cells and materials would affect cell spreading, thus interrupted the interconnection among cells to forming tubes.[9] For example, Shen et al.[42] found that endothelial tube formation proceeded only limited adhesion and was strongly regulated by proline-rich tyrosine kinase 2 (Pyk2). In the present study, on

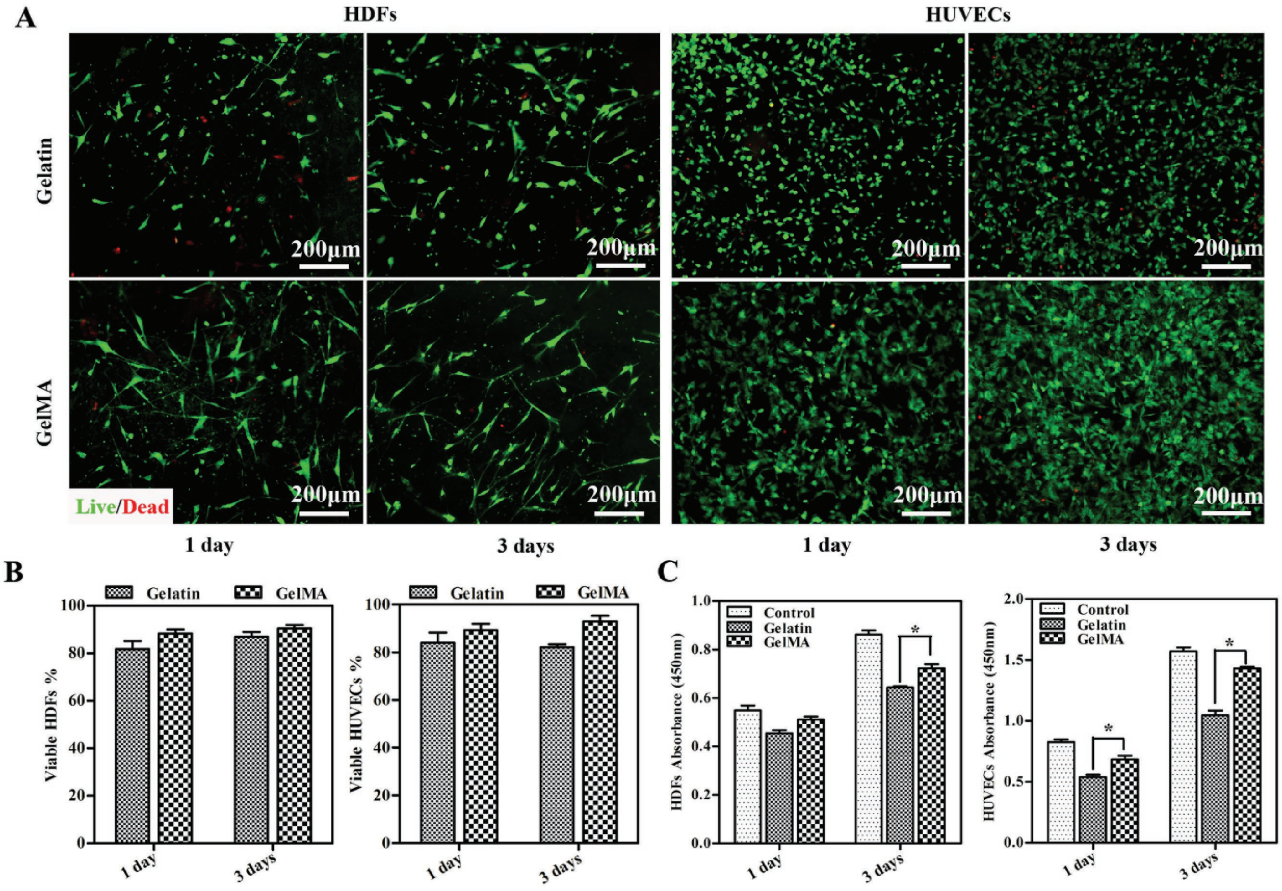

Figure 4. Viability and metabolic activity of cells grown on the electrospun membranes. A) Live/Dead staining of HDFs and HUVECs on crosslinked gelatin and GelMA electrospun membranes on 1 and 3 d. Green fluorescent cells are alive and red fluorescent cells indicate dead cells. B) HDF and HUVEC viability analysis on the electrospun membranes. C) CCK-8 assay of HDF and HUVEC viability after 1 and 3 d culture on the cell culture plate (TCP), crosslinked gelatin, and GelMA membranes. TCP was used as control. *$p < 0.05$ compared with the corresponding controls.

the surface of crosslinked gelatin scaffolds, it was shown that the HDFs and HUVECs had spherical morphology gathering in the pore (Figure 5A). The reason may be that a strong adhesion occurred between the cells and the matrix, preventing the separation of the cell tail and fiber during the process of cell migration. However, HDFs and HUVECs grown into the internal of the GelMA scaffolds and, more importantly, HUVECs connected to each other along the fibers (Figure 5A). Moreover, recent studies have shown that reducing the stiffness of the scaffold would enhance the vessel network formation.[43,44] The results of our study are in conformity with these previous reports. It can be seen that GelMA scaffolds were with softer mechanical stiffness compared with crosslinked gelatin scaffolds. Furthermore, moderate crosslinking methods did not have obvious effect on the structure of the fiber, and convenient crosslinking process could reduce the introduction of harmful substances, which would be harmful to the cells.[45] Our studies showed that the proportion of viable cells on GelMA fibrous scaffolds was higher compared with crosslinked gelatin. Additionally, the results of CCK-8 assay (Figure 4C) also suggested that HDF and HUVEC growth behavior was better on the GelMA fibrous scaffolds. Overall, the cellular suitability of GelMA fibrous scaffold was better than crosslinked gelatin fibrous scaffold in vitro. It is worth noting that by cytoskeleton staining, HUVECs connected to each other along the fibers to form tube structure after 3 d culturing. Based on these results, it indicated that GelMA nanofibrous scaffolds provided a permissive environment for vascular morphogenesis in vitro.

Cell migration, which is related to cell proliferation, cell signaling, and cell-microenvironment interactions, regulates various physiological processes such as vascularization.[46,47] Cell migration was identified as the relative position of cells to the scaffold surface and was calculated using ImageJ software.[48] The mean migration depth was determined as the average depth of the scaffolds, where cells were detected, ignoring the cells on scaffold surface (**Figure 6**). It could be found that cells seeded on the GelMA scaffolds migrated deeper compared with the control crosslinked gelatin scaffolds. After 7 d of cultivation, cells seeded on the GelMA scaffolds migrated to the full depth of the electrospun fibrous scaffolds (100 μm), but the cells on the crosslinked gelatin scaffolds only migrated to 60 μm depth of the fibrous mats. The reason may be due to the fact that the stiffness of the GelMA fibers is lower compared to crosslinked gelatin fibers. It was shown that cells can sense further in a compliable 3D matrix than it in a stiff matrix. Cell migration in a soft 3D matrix is faster compared with that of a

DOI: 10.1002/adfm.201604617

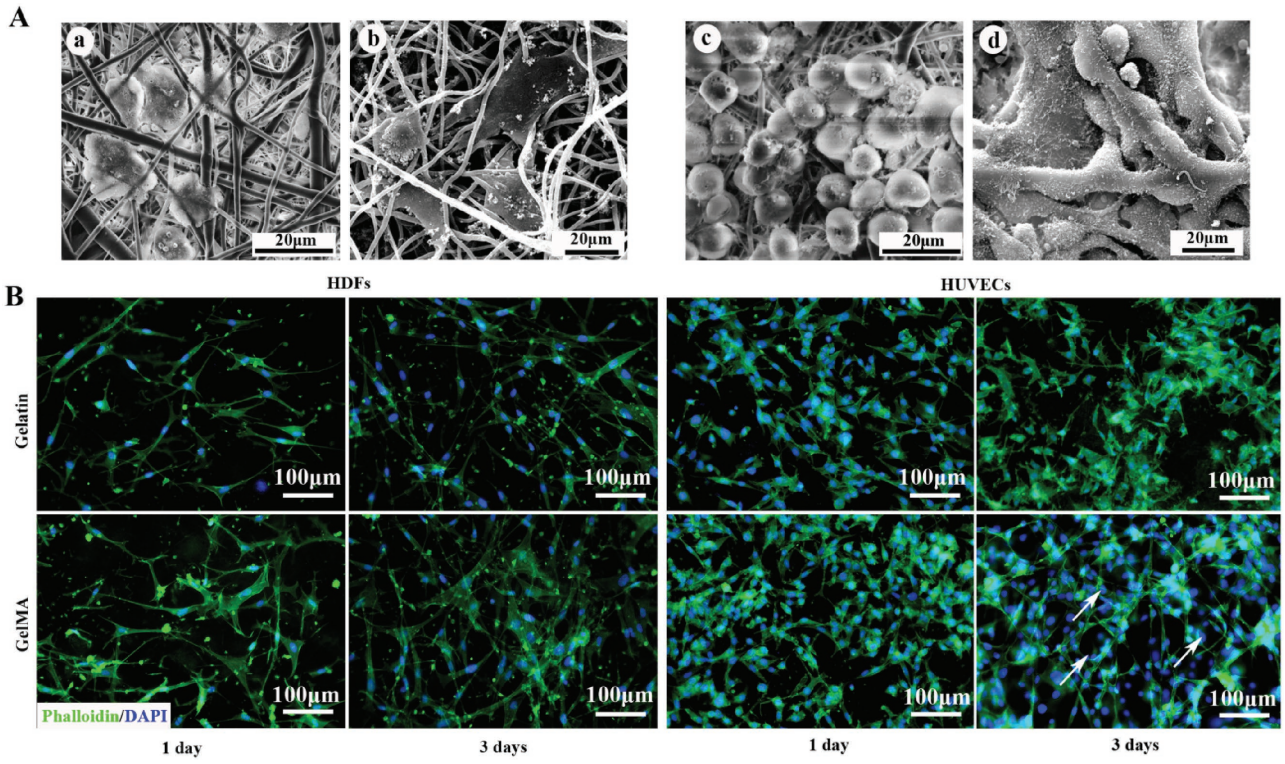

Figure 5. Cells attachment on the electrospun membranes. A) SEM images of HDFs growth on a) the electrospun crosslinked gelatin and b) GelMA fibrous membranes and HUVECs growth on c) the electrospun crosslinked gelatin and d) GelMA fibrous membranes after 3 d of culture. B) Cell filaments are stained with phalloidin (green) and nuclei stained by DAPI (blue).

stiff matrix.[49,50] Also, low fiber stiffness leads to active recruitment of nearby fibers by cells, which increases ligand density on the cell surface and promotes cell adhesion, as well as associated signaling to ultimately facilitate cell migration. The above results demonstrated that a fully cellularized 3D tissue construct was obtained after 7 d of culture of fibroblasts on the GelMA scaffolds, which was expected to be beneficial for in vivo vascularization.

To determine the impact of the electrospun membranes on the cytokine secretion capacity of HDFs for vascularization, HDFs seeded on the membranes and HUVECs seeded on growth factor-reduced Matrigel were co-cultured by transwell plates for detection of HUVEC tubulization capacity. When HDFs were cultured on crosslinked gelatin membrane, HUVECs displayed fewer tubular structures compared with that on GelMA membrane after 12 h (11.8 vs. 40.4 tubules per power field, respectively; $p < 0.05$) (Figure S1A, Supporting Information). To quantify the cytokine secretion for angiogenesis, we performed Enzyme-linked immunosorbent assay (ELISA) on conditioned media from both culture conditions. It was shown that increased protein levels of both basic fibroblast growth factor (bFGF) and vascular endothelial growth factor (VEGF) were found in conditioned media from HDFs on GelMA membrane compared with those seeded on the crosslinked gelatin membrane ($p < 0.05$; Figure S1C, Supporting Information).

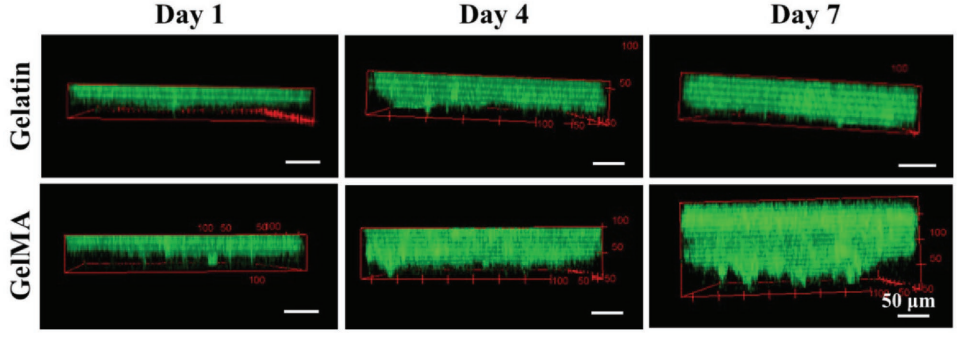

Figure 6. Cell migration into the electrospun scaffolds. Representative images of cell migration into different scaffolds stained using phalloidin (Alexa Fluor 488) for cell filament (green). Scale bars = 50 μm.

2.5. The Influence of Different Electrospun Fibrous Membranes on Flap Viability

All rats survived in the study period. The random skin flaps were treated with two kinds of electrospun fibrous membranes and their necrotic area was analyzed on the seventh postoperative day. Macroscopically, as shown in **Figure 7**A, the regions of necrotic skin were obviously distinguished from the survival flap. The necrotic skin turned into stiff and dark. On postoperative day 7, flap necrosis in the untreated rats was significantly clearer compared with the hydrogel electrospun fibrous membranes treated rats. Additionally, the necrosis

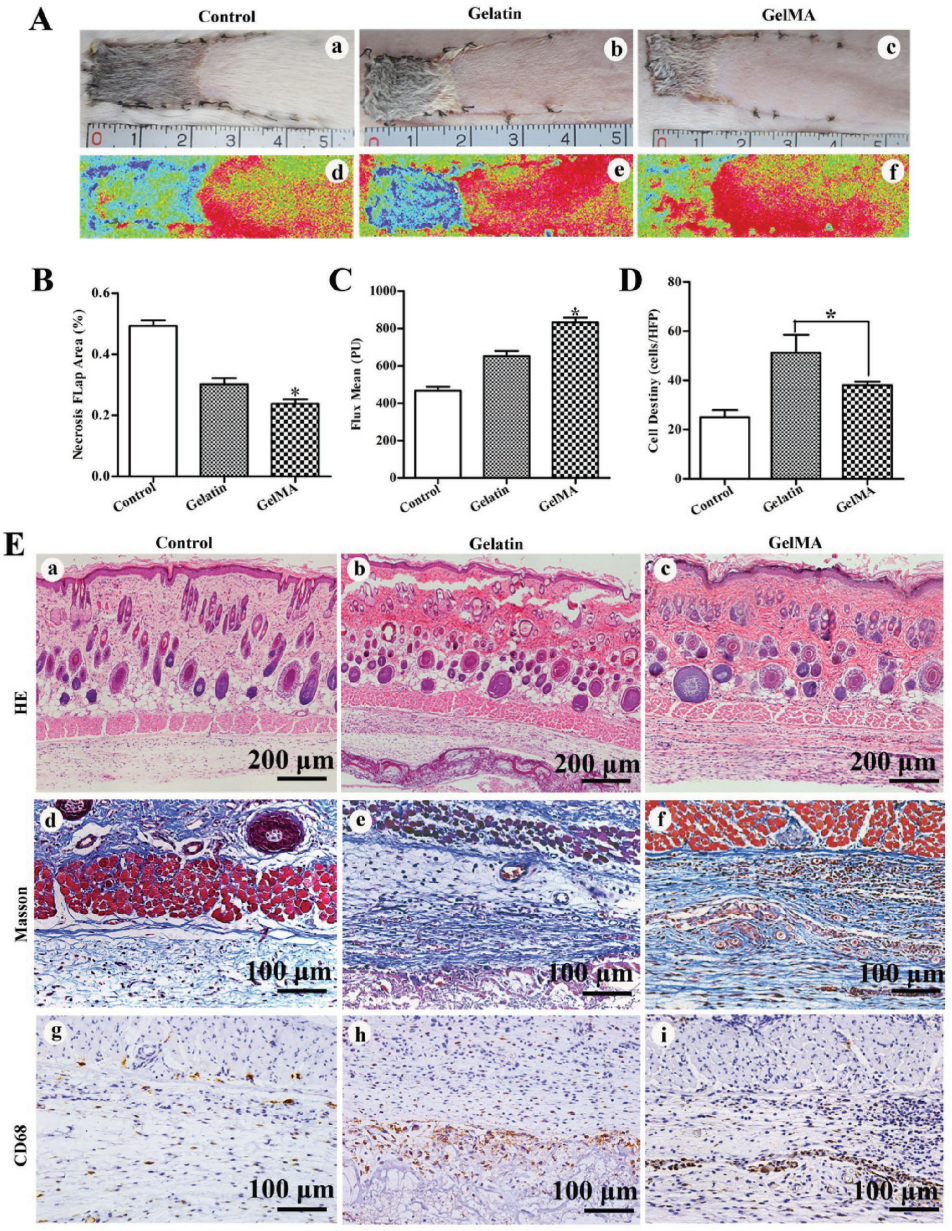

Figure 7. Analysis of necrosis, blood flow perfusion, and inflammatory response of the skin flap after treatment. A) Photographic images of implanting electrospun nanofibrous membranes and photographic images of the skin flap and color laser Doppler detection of skin flaps from the control, crosslinked gelatin, and GelMA groups 7 d postoperation. The color scale illustrates variations in the blood flow, from maximal (red) to minimal perfusion (dark blue). B) The necrosis ratio in the corresponding groups on day 7 after operation. The necrosis ratio was calculated as the area of necrotic tissue/entire area of the flaps ×100% in each sample. C) Quantitative analysis of blood flow perfusion of the flap measured as mean perfusion units ± standard error. D) $CD68^+$ cell density of each group on postoperation day 7. E) Histological analysis of all groups of skin flaps 7 d after surgery. H&E-stained images of all groups: a) control group, b) gelatin group, and c) GelMA group; d) Masson's trichrome staining of the control group, e) gelatin group, and f) GelMA group; immunohistochemical analysis of CD68: g) control group, h) gelatin group, and i) GelMA group; $*p < 0.05$ compared with the corresponding controls.

DOI: 10.1002/adfm.201604617

ratio of the gelatin and GelMA groups was 30.1 ± 4.6% and 23.8 ± 3.3%, respectively. There was a statistically significant difference in necrosis ratio between gelatin and GelMA groups ($p < 0.05$).

To investigate whether the blood supply of the skin flap would be impacted by the different hydrogel electrospun membranes, blood perfusion of skin flap was tested with color laser Doppler imaging system (Figure 7A-d–f). Because of the color laser Doppler imaging system analysis, compared with the control group, hydrogel electrospun membranes caused significant increase in blood flow in the flap tissue on 7 d postoperation. The blood perfusion units (PUs) in group GelMA (832.2 ± 44.0 PU) were significantly higher than that in group gelatin (652.2 ± 48.1 PU), which implied that electrospun GelMA membranes are superior to gelatin membranes in promoting blood perfusion ($p < 0.05$).

As shown in Figure 7E-b, on postoperation day 7, electrospun crosslinked gelatin fibrous membrane was still not fully biodegraded, the structure of which could be clearly observed. However, the GelMA membrane was almost fully biodegraded after 7 d implantation. At the same time, as Figure 7E-c shows, there were more collagen fibers around the electrospun crosslinked gelatin membranes, while the GelMA membrane was replaced by a dermal tissue containing a higher proportion of blood vessels gradually.

To assess the inflammatory response caused by the materials in vivo, anti-CD68 (macrophages) immunohistochemical staining of the sections was used for evaluating the inflammatory cell infiltration into the graft after 7 d postimplantation. It appeared that the hydrogel membranes treatment groups (both crosslinked gelatin and GelMA membrane) contained more positive staining for CD68 cells as compared to the control group (25.0 ± 5.0 cells per high-power-field, HFP); however, higher inflammatory response to macrophages was observed in the crosslinked gelatin group (51.3 ± 12.5 cells per HFP) than in the GelMA group (38.0 ± 2.7 cells per HFP) ($p < 0.05$; Figure 7D). It has been reported that excess inflammation could lead to flap tissue damage in a persistently inflamed state because of ischemia/reperfusion injury.[51,52] Our results demonstrated that less $CD68^+$ cells existed in the implanted electrospun GelMA nanofiber scaffolds after 7 d transplantation. This indicates that the softer and the faster degradation of GelMA nanofiber scaffolds have not caused extensive inflammation.

2.6. The Influence of Different Electrospun Fibrous Membranes on Neovascularization in Ischemic Skin Flaps

In order to assess the effect of different electrospun hydrogel fibrous membranes on the ischemic skin flaps neovascularization, immunofluorescence staining for CD31 was studied by distribution of microvessels in skin flaps. As shown in **Figure 8**B,C, CD31 staining was significantly increased in the flaps treated with GelMA membrane compared with the crosslinked gelatin membrane-treated flaps.

Microvessel density (MVD) was tested by counting the number of the microvessels per hot spot in the section with an antibody reactive to CD31 (Figure 8A–C). Compared with the control (72.0 ± 12.9 microvessels/hot spot) and gelatin (111.4 ± 14.8 microvessels/hot spot) groups, the MVD value in the GelMA group (148.4 ± 19.3 microvessels/hot spot) was the highest among the three groups, 7 d postoperation ($p < 0.05$; Figure 8D). It was observed that there was more microvascular formation after GelMA fibrous scaffold implantation, which was potentially beneficial for the flap tissue.

Finally, despite the above results, it has been known that the degree of crosslinking would affect the properties of the hydrogel. In this study, we did not investigate the different

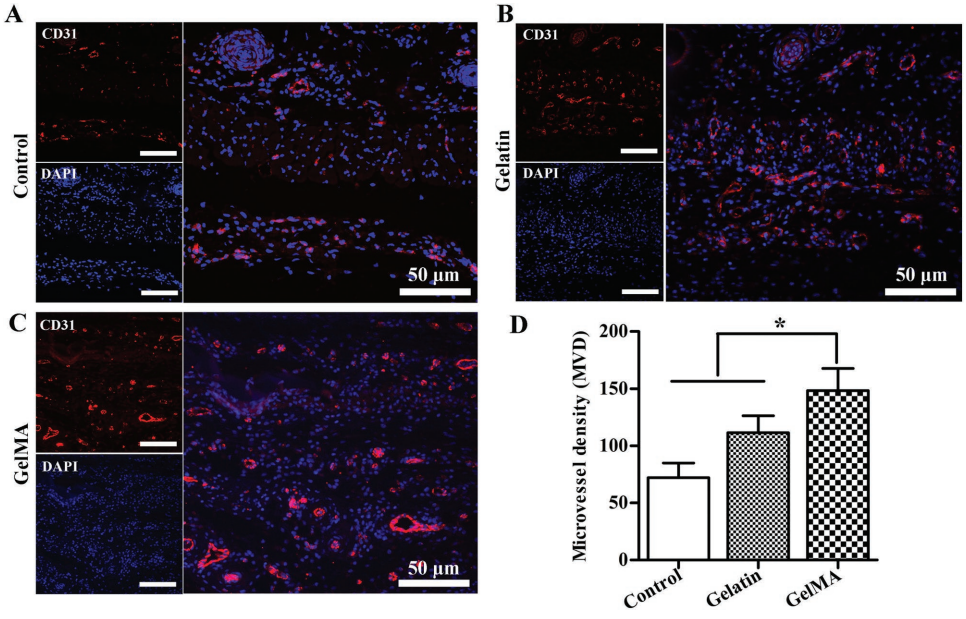

Figure 8. Vascularization. A–C) Immunofluorescence staining of CD31 in the group control, gelatin, and GelMA. D) Microvessel density (MVD) of each group on day 7 postoperation.

levels of crosslinking in the electrospun GelMA system both in vitro and in vivo, which will be studied in our future research for further increasing vascularization, as well as widening its application in the regenerative medicine.

3. Conclusion

In this study, we demonstrated the suitability of scaffolds for accelerated vascularization using a hydrogel based on photocrosslinkable gelatin (GelMA) by electrospinning. We also demonstrated that electrospun GelMA nanofiber scaffolds can support cell adhesion, proliferation, migration in vitro, and formation of 3D vascular networks in vivo. Due to the benefits that photocrosslinkable gelatin can provide, including controllable mechanical and degradation properties, the resultant electrospun nanofibrous scaffolds can provide rapid regeneration and formation of cutaneous tissues with less inflammation compared with crosslinked gelatin nanofibrous. In summary, we propose that GelMA nanofiber scaffold is a particularly promising candidate for skin tissue regeneration that required the formation of functional vascular in future.

4. Experimental Section

Materials: Gelatin (porcine skin, type-A powder) and MA were purchased from Sigma (St. Louis, MO). All other chemicals and solvents were of reagent grade and purchased from Guoyao Regents Company (Shanghai, P. R. China).

Fabrication of Electrospun Fibrous Scaffolds—Gelatin Electrospun Fibers: 100 mg of gelatin A from porcine skin (Sigma-Aldrich, St. Louis, MO) was totally dissolved in 1 mL of HFIP. The solution was then filled into a syringe and put in a syringe pump (Harvard, MA) that was attached to a high-voltage statitron. An aluminum foil collector plate (30 cm × 30 cm square plate) was used on the anode. An oblong counter electrode was located about 15 cm from the capillary tip, with the voltage at 20 kV between the source and the collector plate. The polymer solution was pumped out at a rate of 4 mL h^{-1}, and 1 g of gelatin was used to spin each sheet. After electrospinning, the gelatin was chemically crosslinked. The gelatin electrospun fibers were stored in ethanol with 2% of glutaraldehyde for crosslinking. After overnight, the electrospun sheets were immersed in the 1.5% of glycine solution to wash away the glutaraldehyde.

Fabrication of Electrospun Fibrous Scaffolds—GelMA Electrospun Fibers: Electrospinning GelMA fibers were fabricated following the same protocol as that of gelatin fibers. The electrospun GelMA sheets were photocrosslinked upon UV light exposure. To prepare the photocrosslinking solution, 1.0 g 2-hydroxy-4′-(2-hydroxyethoxy)-2-methylpropiophenone (photoinitiator, Irgacure 2959, Sigma-Aldrich, St. Louis, MO) was added to 10 mL of ethanol in the absence of light and stirred until completely dissolved. Uncrosslinked electrospun GelMA fibers were immersed in the photocrosslinking solution and exposed to 365 nm UV light (Select XLE-Series UV crosslinker, XL-1000A) for 30 min. The crosslinked GelMA fibers were then subject to DI wash to remove excess photoinitiator.

Physical Characterization of Hydrogel Electrospun Fibrous Scaffolds—SEM-Based Fiber Diameter: The morphology of the fibrous scaffolds was examined by SEM (FEI Quanta 250, the Netherlands). The dry scaffolds were placed in a dry container overnight to ensure they were completely free of moisture. Dry samples were then sputter coated with gold (Model 550; Electron Microscope Sciences) in preparation for SEM. SEM images of each sample were taken at 2000× and 5000× magnification. In addition, samples of each dry electrospun scaffold were placed in PBS for 24 h, and then SEM images of these hydrated samples were taken at 2000× and 5000× after freeze drying. To determine the fiber diameter, the SEM images at 5000× magnification were taken. From each image, at least 60 different fibers and 300 different segments were randomly selected to measure the average fiber diameter using Photoshop. An average fiber diameter was determined by measuring the diameter of 60 different fibers. The same procedure was used for SEM of both the dry and hydrated scaffolds.

Physical Characterization of Hydrogel Electrospun Fibrous Scaffolds—Water Retention: The weight of the samples before and after 24 h water immersion was recorded as W_D and W_0, respectively. Samples were then left in air at room temperature and the weight (W_t) was measured at pre-determined time points.[47] The water sorption, SR, at time t was calculated according to the following equation[53]

$$SR = \frac{W_t - W_D}{W_D} \times 100\% \quad (1)$$

Physical Characterization of Hydrogel Electrospun Fibrous Scaffolds—Water Vapor Permeability: To examine the water vapor permeability of the nanofibers, the crosslinked gelatin and GelMA nanofibers were separately stuck on the ends of 17 × 60 mm (o.d. × H) Glass Threaded Vials (Fisher, MA), containing 6 mL of Dulbecco's phosphate buffered saline (DPBS). The vials were placed at 37 °C and weighed every 24 h to determine the water loss.[54]

Physical Characterization of Hydrogel Electrospun Fibrous Scaffolds—Water Permeability: The method for permeability experiments was used as previously described elsewhere.[54] Briefly, after placing the scaffolds into separate water-tight specimen mounts, the specimen mount was connected with a three-way stop/start valve to one and two pipettes. The latter was positioned near horizontally. Once the mount was filled, the water level was kept at 100–105 cm. The 5 cm difference could be considered negligibly.

Electrospun scaffolds were soaked in DI water before 1 h water permeability experiments. The thickness of the swollen scaffold was measured using a caliper. The scaffolds were loaded into the specimen mount using a cross-sectional area of 0.7 cm^2 with the tubing filling with DI water. The valve was opened to allow free water flow after recording the initial volume on the pipette. After 5 min, the volume of the pipette was recorded again, which was determined to be the cutoff time points after which water flow decreased for each sample. Each material type was tested at least three times.

According to Darcy's Law, permeability (k) was calculated with the formula below[54]

$$k = Q\eta h/Ftp \quad (2)$$

where k is the permeability of the specimen in Darcy's units (D), Q is the volume of fluid that permeated the specimen at time t, η is the fluid viscosity (in our study, 0.89 cp for water at 25 °C), h is the specimen thickness, F is the cross sectional area of the specimen, which is perpendicular to fluid flow direction, and p is the applied pressure head.

Physical Characterization of Hydrogel Electrospun Fibrous Scaffolds—Tensile Testing: For mechanical property tests, the electrospun fibrous scaffolds were left to soak in DI water for 1 h before testing. Then, electrospun fibrous scaffolds were punched into small strips (30.0 × 10.0 mm^2). The thickness was calculated as the averaged measurement using a caliper at the lengthwise ends and the center. Uniaxial tensile tests were performed using Instron 5567 (Norwood, MA) mechanical tester. The samples were loaded with around length of 20 mm between the clamps. For tensile testing, the samples were stretched until failure at the elongation rate of 10 mm min^{-1}. From the stress–strain curves, Young's modulus, tensile strength, and elongation at break of the scaffolds were obtained.

Physical Characterization of Hydrogel Electrospun Fibrous Scaffolds—Degradation in Vitro: The degradation properties of crosslinked gelatin and GelMA fibrous scaffolds were determined in DI water at 37 °C. The percentage of weight loss was determined at different time by the ratio of the mass to the original mass.

Ethical Statements: HDFs were isolated from human normal skin obtained from the Department of Plastic and Reconstructive Surgery, Ninth People's Hospital Affiliated to Medical School of Shanghai Jiao Tong University (Shanghai, China). This study protocol was approved

DOI: 10.1002/adfm.201604617

by the Ethical Committee of Shanghai Ninth People's Hospital Affiliated Shanghai Jiao Tong University School of Medicine. The animal experiments were in accordance with international ethics guidelines and the National Institutes of Health Guide concerning the Care and Use of Laboratory Animals.

In Vitro Viability and Proliferation: To assess HDF and HUVEC viability after hydrogel membrane seeding, a Live/Dead cell viability assay was performed, according to the manufacturer's instructions (Life Technologies), at different time points.

HDF and HUVEC proliferation on different membranes was analyzed by a Cell Counting Kit-8 (Dojindo) on 1 d and 3 d. The cell-membrane samples were washed three times with PBS after culture medium removal, and then 1000 µL of culture medium was added in each well. 100 µL of CCK-8 reagent was added to each sample and incubated at 37 °C for 2 h. 100 µL of incubated medium of each well was transferred to a 96-well culture plate, and then the absorbance intensity of each sample was measured at a wavelength of 450 nm using a microplate reader (Thermo Labsystems, USA). All experiments were repeated three times.

Cell Morphology and Attachment: Imaging of HUVECs seeded on crosslinked gelatin and GelMA electrospun nanofibrous membranes after 3 d with SEM was performed, as described elsewhere.[55] In brief, membranes were washed with PBS three times following fixation with 4% glutaraldehyde for 2 h at 4 °C. After that, the samples were dehydrated by a standard ethanol series followed by three-time wash with PBS. After coated with gold, specimens were observed by SEM.

To analyze the cells adhesion on the fibrous membranes, HDF and HUVEC adhesion on the membranes was observed after staining with phalloidin-FITC (Sigma) and 4,6-diamidino-2-phenylindle (DAPI) at 1 and 3 d, respectively. The culture medium was removed and the cell membrane samples were fixed in 4% paraformaldehyde for 20 min at room temperature, following an extensive wash in PBS for three times. Cells were permeabilized with 0.1% Triton X-100 for 20 min and washed again in PBS. And then, the cells were blocked in 1% albumin bovine serum (BSA) in PBS for 45 min. Cells were stained with a 50 mg mL^{-1} fluorescent phalloidin conjugate solution in PBS. Cell nuclei were stained with DAPI. Fluorescent images were then acquired using a fluorescence microscope (Zeiss, NY).

Matrigel Tubulization Assays and Cell Secretion: To study the effects of different electrospun nanofibrous membranes on cell secretion, as well as to test the role of vascularization, crosslinked gelatin and GelMA membranes carrying HDFs were taken out after 3 d culturing, followed by rinsing repeatedly. After that, two kinds of membranes carrying HDFs were embedded into the upper chamber of the insert (transwell plates were 12 mm in diameter with 0.4 µm pore filters, Corning Costar, Cambridge, MA) with 400 µL of serum-free culture medium. Calcein-labeled HUVECs were seeded on a 12-well plate (10^5 cells per well) coated with growth factor-reduced Matrigel (BD Biosciences) with 1000 µL of culture medium without serum. After 6 and 12 h, the number of HUVEC tubules was counted in three random low-power fields per well by using an inverted microscope. Conditioned media was collected from HDFs seeded onto electrospun hydrogel nanofibrous membranes; protein levels of VEGF and bFGF were quantified using the Human VEGF and FGF basic Quantikine ELISA Kit (Excell Bio, Shanghai, China).

Macroscopic Evaluation and Skin Blood Perfusion: At day 7 of treatment, the animals were anaesthetized and the surviving and necrotic areas of the flaps were photographed with a digital camera. The survival and necrosis of flaps were defined with respect to the gross appearance, texture, and tissue elasticity. The necrotic area was quantified as a percentage of the total flap area and the results were expressed as percentages of skin necrosis. These defined surface areas were measured by Image-Pro Plus version 6.0 software.

Blood perfusion of the skin flap was assessed on day 7 with a laser Doppler flowmetry (Moor Instruments, Axminster, UK) and was quantified using the laser Doppler imager at controlled temperature (28–30 °C). Laser Doppler perfusion imaging was assessed according to the following parameters: a display rate of 25 Hz, time constant of 1.0 s, and camera exposure time of 20 ms. Results were recorded as blood PU.

Histology Analysis: On day 7 postoperation, each 1 × 1.5 cm similar position of flap specimen was harvested for a histological assessment. All tissue samples were fixed with 4% neutral formalin for at least 24 h, embedded in paraffin, cross-sectioned along the tissue into 5 µm slices, and stained using hematoxylin–eosin (H&E) and Masson's trichrome for light microscopy.

Detection of Inflammatory Response: Consecutive specimens (5 µm) were done from the paraffin-embedded tissues for immunohistochemical analysis of inflammatory response. Briefly, after deparaffinization using xylene and ethanol, endogenous peroxidase activity was blocked with 3% of H_2O_2 for 10 min and rinsed in PBS, and 5% of BSA blocking solution was applied for 10 min. The primary antibody against CD68 (Abcam, US), which was diluted 1:100 in PBS, was applied at 4 °C overnight. The next day, the sections were rinsed in PBS and incubated with an horseradish peroxidase (HRP)-conjugated secondary goat-anti-rat antibody. Results were observed and photographed using a microscope (Nikon, Japan) connected to a digital camera.

To observe macrophage infiltration, the expression of $CD68^+$ cell intensive regions under low magnification was searched and the density was valued in five random horizons per specimen at 200× magnification by selecting five different areas. The number of $CD68^+$ cells was counted. The average cell number in five different areas was considered as the value of cell density. All counts were performed by three different researchers blinded to the samples.

Detection of Vascularization and MVD: Specimens were embedded in optimal cutting temperature compound (OCT) and frozen in liquid nitrogen for fluorescent immunostaining. 7 µm thick frozen sections were blocked in 10% normal goat serum/0.05% Triton X-100/0.2% BSA (Sigma) in PBS for 40 min at room temperature. The sections were incubated overnight at 4 °C with a primary antibody (PECAM1/CD31, Santa Cruz Biotechnology, Inc), followed by incubation with goat anti-mouse IgG-TR (Texas Red) secondary antibody for 1 h at 37 °C. DAPI (Sigma) was used to stain nuclei for 10 min. Subsequently, sections were imaged with fluorescence microscopy.

MVD was assessed in the chosen fields with the three hot spots (the most vascularized areas) under 200× magnification for each specimen. Subsequently, the microvessel numbers were counted at 400× magnification within the hot spot area. Only the vessels with clear clusters of endothelial cells with lumen were counted. The MVD value was defined as the average vessel count in three hot spots. All counts were performed by three investigators blinded to the samples.

Statistical Analysis: The data differences were analyzed by ANOVA with a post hoc Dunn or Bonferroni test. Data were presented as mean ± standard deviation. All the data were processed using IBM SPSS Statistics 19 for Windows. A value of $p < 0.05$ was considered to be statistically significant.

Supporting Information

Supporting Information is available from the Wiley Online Library or from the author.

Acknowledgements

X.S., Q.L., and H.Z. contributed equally to this work. This work was supported in part by the National Natural Science Foundation of China (51373112 and 81372073), Jiangsu Provincial Special Program of Medical Science (BL2012004), Jiangsu Provincial Clinical Orthopedic Center, and the Priority Academic Program Development of Jiangsu Higher Education Institutions (PAPD). Dr. Zhang acknowledges financial support from Jane and Aatos Erkko Foundation (Grant No. 4704010). Dr. H. A. Santos acknowledges financial support from the Academy of Finland (Decision Nos. 252215 and 281300), the University of Helsinki Research Funds, the Biocentrum Helsinki, and the European Research

Council under the European Union's Seventh Framework Programme (FP/2007-2013, Grant No. 310892).

Received: September 6, 2016
Published online:

[1] L. R. Estevão, J. P. Medeiros, L. Baratella-Evêncio, R. S. Simões, Fde. S. Mendonça, J. Evêncio-Neto, *Acta Cir. Bras.* **2013**, *28*, 863.
[2] J. P. Barret, D. N. Herndon, R. L. McCauley, *Burns* **2002**, *28*, 500.
[3] M. Buemi, M. Galeano, A. Sturiale, R. Ientile, C. Crisafulli, A. Parisi, M. Catania, G. Calapai, P. Impalà, C. Aloisi, F. Squadrito, D. Altavilla, A. Bitto, G. Tuccari, N. Frisina, *Shock* **2004**, *22*, 169.
[4] A. Ozturk, C. Fırat, H. Parlakpınar, A. Bay-Karabulut, H. Kirimlioglu, A. Gurlek, *Exp. Diabetes Res.* **2012**, *2012*, 721256.
[5] M. Yang, L. Sheng, H. Li, R. Weng, Q. Li, *Microsurgery* **2010**, *30*, 275.
[6] M. M. Pavletic, *Vet. Q.* **1997**, *19*, 24.
[7] A. Kampmann, D. Lindhorst, P. Schumann, R. Zimmerer, H. Kokemüller, M. Rücker, N. C. Gellrich, F. Tavassol, *Microvasc. Res.* **2013**, *90*, 71.
[8] H. J. Chung, J. T. Kim, H. J. Kim, H. W. Kyung, P. Katila, J. H. Lee, T. H. Yang, Y. I. Yang, S. J. Lee, *J. Controlled Release* **2015**, *205*, 218.
[9] X. Sun, R. Zheng, L. Cheng, X. Zhao, R. Jin, L. Zhang, Y. Zhang, Y. Zhang, W. Cui, *RSC Adv.* **2016**, *6*, 9360.
[10] R. Gemperli, A. M. Munhoz, *Acta Cir. Bras.* **2013**, *28*, 487.
[11] S. Eghtesad, M. V. Nurminskaya, *J. Biomater. Sci. Polym. Ed.* **2013**, *24*, 2006.
[12] S. H. Ku, C. B. Park, *Biomaterials* **2010**, *31*, 9431.
[13] M. Patenaude, N. M. Smeets, T. Hoare, *Macromol. Rapid Commun.* **2014**, *35*, 598.
[14] G. D. Nicodemus, S. J. Bryant, *Tissue Eng. Part B: Rev.* **2008**, *14*, 149.
[15] Z. Y. Lin, V. Shah, A. Dhinakar, L. Yildirimer, W. G. Cui, X. Zhao, *Plastic Aesthetic Res.* **2016**, *3*, 72.
[16] L. Cheng, X. Sun, M. Tang, R. Jin, W. Cui, Y. Zhang, *Plastic Aesthetic Res.* **2016**, *3*, 92.
[17] J. W. Nichol, S. T. Koshy, H. Bae, C. M. Hwang, S. Yamanlar, A. Khademhosseini, *Biomaterials* **2010**, *31*, 5536.
[18] S. T. Koshy, T. C. Ferrante, S. A. Lewin, D. J. Mooney, *Biomaterials* **2014**, *35*, 2477.
[19] X. Zhao, Q. Lang, L. Yildirimer, Z. Y. Lin, W. G. Cui, N. Annabi, K. W. Ng, M. R. Dokmeci, A. M. Ghaemmaghami, A. Khademhosseini, *Adv. Healthcare Mater.* **2016**, *5*, 108.
[20] Y. C. Chen, R. Z. Lin, H. Qi, Y. Yang, H. Bae, J. M. Melero-Martin, A. Khademhosseini, *Adv. Funct. Mater.* **2012**, *22*, 2027.
[21] A. J. Rufaihah, D. Seliktar, *Adv. Drug Delivery Rev.* **2016**, *96*, 31.
[22] H. Naderi, M. M. Matin, A. R. Bahrami, *J. Biomater. Appl.* **2011**, *26*, 383.
[23] O. C. Velazquez, *J. Vasc. Surg.* **2007**, *45*, A39.
[24] A. H. Van Hove, K. Burke, E. Antonienko, E. Brown, D. S. Benoit, *J. Controlled Release* **2015**, *217*, 191.
[25] K. C. Kuo, R. Z. Lin, H. W. Tien, P. Y. Wu, Y. C. Li, J. M. Melero-Martin, Y. C. Chen, *Acta Biomater.* **2015**, *27*, 151.
[26] P. Allen, J. Melero-Martin, J. Bischoff, *J. Tissue Eng. Regenerative Med.* **2011**, *5*, e74.
[27] G. E. Davis, D. R. Senger, *Circulation Res.* **2005**, *97*, 1093.
[28] H. K. Kleinman, G. R. Martin, *Seminars Cancer Biol.* **2005**, *15*, 378.
[29] C. Helary, I. Bataille, A. Abed, C. Illoul, A. Anglo, L. Louedec, D. Letourneur, A. Meddahi-Pelle, M. M. Giraud-Guille, *Biomaterials* **2010**, *31*, 481.
[30] B. J. Klotz, D. Gawlitta, A. J. Rosenberg, J. Malda, F. P. Melchels, *Trends Biotechnol.* **2016**, *34*, 394.
[31] K. Yue, G. Trujillo-de Santiago, M. M. Alvarez, A. Tamayol, N. Annabi, A. Khademhosseini, *Biomaterials* **2015**, *73*, 254.
[32] H. K. Cheung, T. T. Han, D. M. Marecak, J. F. Watkins, B. G. Amsden, L. E. Flynn, *Biomaterials* **2014**, *35*, 1914.
[33] M. Fartasch, *Curr. Probl. Dermatol.* **1995**, *23*, 95.
[34] H. Doyle, S. Lohfeld, P. McHugh, *Med. Eng. Phys.* **2015**, *37*, 767.
[35] S. Zhao, J. Zhao, S. Dong, X. Huangfu, B. Li, H. Yang, J. Zhao, W. Cui, *Int. J. Nanomed.* **2014**, *9*, 2373.
[36] D. S. Thoma, C. C. Villar, D. L. Cochran, C. H. Hämmerle, R. E. Jung, *Clin. Oral Implants Res.* **2012**, *23*, 1333.
[37] K. Wingate, W. Bonani, Y. Tan, S. J. Bryant, W. Tan, *Acta Biomater.* **2012**, *8*, 1440.
[38] Y. Xu, M. Fu, Z. Li, Z. Fan, X. Li, Y. Liu, P. M. Anderson, X. Xie, Z. Liu, J. Guan, *Acta Biomater.* **2016**, *31*, 99.
[39] S. Lee, C. M. Valmikinathan, J. Byun, S. Kim, G. Lee, N. Mokarram, S. B. Pai, E. Um, R. V. Bellamkonda, Y. S. Yoon, *Biomaterials* **2015**, *63*, 158.
[40] A. S. Sawhney, C. P. Pathak, J. J. van Rensburg, R. C. Dunn, J. A. Hubbell, *J. Biomed. Mater. Res.* **1994**, *28*, 83.
[41] X. Zhao, I. Olsen, H. Li, K. Gellynck, P. G. Buxton, J. C. Knowles, V. Salih, A. M. Young, *Acta Biomater.* **2010**, *6*, 845.
[42] C. J. Shen, S. Raghavan, Z. Xu, J. D. Baranski, X. Yu, M. A. Wozniak, J. S. Miller, M. Gupta, L. Buckbinder, C. S. Chen, *Exp. Cell Res.* **2011**, *317*, 1860.
[43] M. D. Stevenson, H. Piristine, N. J. Hogrebe, T. M. Nocera, M. W. Boehm, R. K. Reen, K. W. Koelling, G. Agarwal, A. L. Sarang-Sieminski, K. J. Gooch, *Acta Biomater.* **2013**, *9*, 7651.
[44] A. Lesman, D. Rosenfeld, S. Landau, S. Levenberg, *Adv. Drug Delivery Rev.* **2016**, *96*, 176.
[45] M. A. Azagarsamy, K. S. Anseth, *ACS Macro Lett.* **2013**, *2*, 5.
[46] T. S. Deisboeck, I. D. Couzin, *BioEssays* **2009**, *31*, 190.
[47] P. Rorth, *Annu. Rev. Cell Dev. Biol.* **2009**, *25*, 407.
[48] C. Schmitz, B. S. Eastwood, S. J. Tappan, J. R. Glaser, D. A. Peterson, P. R. Hof, *Front. Neuroanat.* **2014**, *8*, 27.
[49] P. Soman, J. A Kelber, J. W. Lee, T. N. Wright, K. S. Vecchio, R. L. Klemke, S. Chen, *Biomaterials* **2012**, *33*, 7064.
[50] A. Buxboim, I. L. Ivanovska, D. E. Discher, *J. Cell Sci.* **2010**, *123*, 297.
[51] H. J. Kim, L. Xu, K. C. Chang, S. C. Shin, J. I. Chung, D. Kang, S. H. Kim, J. A. Hur, T. H. Choi, S. Kim, J. Choi, *Microsurgery* **2012**, *32*, 563.
[52] A. Can, M. Temel, R. Dokuyucu, M. Mutaf, *Ann. Plast. Surg.* **2016**, *77*, e9.
[53] K. K. Nayak, P. Gupta, *Int. J. Biol. Macromol.* **2015**, *81*, 1.
[54] S. Sell, C. Barnes, D. Simpson, G. Bowlin, *J. Biomed. Mater. Res. A* **2008**, *85*, 115.
[55] L. Cheng, X. Sun, B. Li, C. Hu, H. Yang, Y. Zhang, W. Cui, *J. Mater. Chem. B* **2013**, *1*, 4428.